

Activation of the CREB Coactivator CRTC2 by Aberrant Mitogen Signaling promotes oncogenic functions in HPV16 positive head and neck cancer



Miranda B. Carper^a; Saumya Goel^{b,c};
Anna M. Zhang^b; Jeffrey S. Damrauer^a;
Stephanie Cohen^d; Matthew P. Zimmerman^e;
Gabrielle M. Gentile^e; Kshitij Parag-Sharma^f;
Ryan M. Murphy^g; Kotaro Sato^{h,i};
Kwangok P. Nickel[†]; Randall J. Kimple[†];
Wendell G. Yarbrough^{h,i,k}; Antonio L. Amelio^{l,m,n,*}

^a Lineberger Comprehensive Cancer Center, UNC School of Medicine, The University of North Carolina at Chapel Hill, NC, USA

^b Oral and Craniofacial Health Sciences, Adams School of Dentistry, The University of North Carolina at Chapel Hill, NC, USA

^c Carolina Research Scholar, Undergraduate Curriculum in Biochemistry, The University of North Carolina at Chapel Hill, NC, USA

^d Pathology Services Core, Lineberger Comprehensive Cancer Center, UNC School of Medicine, The University of North Carolina at Chapel Hill, Chapel Hill, NC, USA

^e Graduate Curriculum in Genetics & Molecular Biology, Biological & Biomedical Sciences Program, UNC School of Medicine, The University of North Carolina at Chapel Hill, NC, USA

^f Graduate Curriculum in Cell Biology & Physiology, Biological & Biomedical Sciences Program, UNC School of Medicine, The University of North Carolina at Chapel Hill, NC, USA

^g Graduate Curriculum in Pharmacology, Biological & Biomedical Sciences Program, UNC School of Medicine, The University of North Carolina at Chapel Hill, NC, USA

^h Department of Oral and Maxillofacial Surgery, Graduate School of Medicine, Nagoya University, Nagoya, Japan

ⁱ Department of Human Oncology and UW Carbone Cancer Center, School of Medicine and Public Health, University of Wisconsin, Madison, WI, USA

^j Department of Otolaryngology/Head and Neck Surgery, University of North Carolina School of Medicine, Chapel Hill, North Carolina, Chapel Hill, NC, USA

^k Department of Pathology, University of North Carolina School of Medicine, Chapel Hill, North Carolina, Chapel Hill, NC, USA

^l Department of Cell Biology and Physiology, UNC School of Medicine, University of North Carolina at Chapel Hill, Chapel Hill, NC, USA

^m Biomedical Research Imaging Center, UNC School of Medicine, The University of North Carolina at Chapel Hill, NC, USA

ⁿ Lineberger Comprehensive Cancer Center, Cancer Cell Biology Program, UNC School of Medicine, University of North Carolina at Chapel Hill, Chapel Hill, NC, USA

Abstract

Head and neck squamous cell carcinoma (HNSCC) is the 6th most common cancer worldwide and incidence rates are continuing to rise globally. Patients often present with locally advanced disease and a staggering 50% chance of relapse following treatment. Aberrant activation of adaptive response signaling pathways, such as the cAMP/PKA pathway, induce an array of genes associated with known cancer pathways that promote tumorigenesis and drug resistance. We identified the cAMP Regulated Transcription Coactivator 2 (CRTC2) to be overexpressed and constitutively activated in HNSCCs and this confers poor prognosis. CRTCs are regulated through their subcellular localization and we show that CRTC2 is exclusively nuclear in HPV(+) HNSCC, thus constitutively active, due to non-canonical Mitogen-Activated Kinase Kinase 1 (MEKK1)-mediated activation via a MEKK1-p38 signaling axis. Loss-of-function and pharmacologic inhibition experiments decreased CRTC2/CREB transcriptional activity by reducing nuclear CRTC2 via nuclear import inhibition and/or by eviction of CRTC2 from the nucleus. This shift in localization was associated with decreased proliferation,

* Corresponding author.

E-mail address: antonio_amelio@unc.edu (A.L. Amelio).

Received 31 December 2021; received in revised form 14 April 2022; accepted 14 April 2022

migration, and invasion. Our results suggest that small molecules that inhibit nuclear CRTC2 and p38 activity may provide therapeutic benefit to patients with HPV(+) HNSCC.

Neoplasia (2022) 29, 100799

Keywords: Head and neck cancer, CREB, cAMP Regulated transcription coactivators, HPV(+) oropharyngeal cancer

Introduction

Cancers that arise in squamous cells lining mucosal surfaces of the head and neck region are collectively referred to as head and neck squamous cell carcinomas (HNSCCs). Nearly 700,000 new HNSCC cases are diagnosed annually worldwide, and this is accompanied by more than 300,000 deaths [1]. A majority of HNSCC patients present with locally advanced disease and a staggering 50% chance of relapse following treatment [2]. Etiologic factors for developing HNSCC include the consumption of tobacco and alcohol, and high-risk human papillomavirus (HPV) infections [2,3]. While HNSCC cancers associated with tobacco and alcohol consumption are decreasing in the developing world, the incidence of HPV-induced HNSCC is steadily increasing and is implicated in over 70% of all oropharyngeal carcinomas in the United States [4,5]. Interestingly, HNSCCs exhibit significant molecular heterogeneity despite commonly arising within the mucosal epithelia of the upper aerodigestive tract suggesting that a better understanding of the molecular landscape and signaling pathways involved is needed.

Aberrant activation of kinase cascades, such as mitogen activated protein kinases (MAPK), cAMP/PKA, RSK2, and AKT signaling pathways, commonly occurs in cancer [6,7]. The master transcription factor cAMP Response Element Binding protein (CREB) lies directly downstream of these signal transduction regulators and induces transcription of a multitude of adaptive response gene targets including those involved in glucose metabolism, cell growth, survival, angiogenesis, immune evasion, and the maintenance of tumor stem cells [6–10]. Consequently, CREB is activated in a variety of tumors including lung, breast, prostate, kidney, ovarian, gastric, esophageal, pancreatic, and head and neck cancers although the mechanisms controlling CREB activity varies widely [6,7,10–14]. For example, canonical CREB phosphorylation (Ser133) induces expression of target genes with promoters containing cAMP response elements (CRE), but CREB phosphorylation alone does not always correlate with increased target gene expression. In fact, physical interactions between CREB and the cAMP-Regulated Transcriptional Coactivators (CRTCs) are essential for target gene regulation [9,15].

There are three CRTC family members (CRTC1-3) each with varying expression in different tissue types. Notably, CRTCs are dysregulated in a variety of cancers including esophageal squamous cell, colorectal, non-small cell lung (NSCL), and mucoepidermoid salivary gland carcinomas (MEC) by overexpression, mutation, gene fusions, and/or disruption of upstream negative regulators such as the tumor suppressor LKB1 (*STK11*) [9,16–20]. CRTCs are normally phosphorylated by salt inducible kinases (SIKs) and sequestered in the cytoplasm via 14-3-3 proteins until cAMP/Ca²⁺ signaling induces CRTC de-phosphorylation and shuttling to the nucleus where they bind and stimulate CREB transcriptional activity [9]. Therefore, CRTC phosphorylation is generally understood to sequester CRTCs to the cytoplasmic compartment and prevent its binding to nuclear CREB. However, several reports suggest that CRTC activation can be stimulated by non-canonical phosphorylation events mediated by mitogen signals. Specifically, Sonntag et al. found that the phosphorylation of CRTC3

on Ser391 by cyclin dependent kinases and the MAPK/ERK induces the recruitment of PP2A and the subsequent dephosphorylation of inhibitory 14-3-3 binding sites (Ser162 and Ser273), thereby resulting in nuclear translocation of CRTC3 [21]. Similarly, Siu et al. revealed that MEKK1 induced non-canonical phosphorylation of CRTC1 (i.e., not the 14-3-3 binding sites at Ser167 and Ser 261) promotes nuclear translocation rather than eviction, and subsequently increased CREB target gene expression [22]. However, the impact of non-canonical phospho-CRTC2 regulation and its effects on CREB-driven oncogenesis remain poorly understood.

Here, we identify CRTC2 as a key transcriptional co-regulator of CREB in HNSCCs. We show that CRTC2 confers poor prognosis in HPV positive (HPV(+)) HNSCCs. Constitutive nuclear localization of CRTC2 and subsequent CREB activation are regulated in HPV(+) HNSCCs by aberrant MEKK1-mediated mitogen signaling. Collectively, these studies demonstrate the importance of the CREB-CRTC2 pathway in linking gain-of-function MEKK1 activation in HPV(+) HNSCC to oncogenesis.

Materials and methods

Bioinformatics

Bioinformatics analyses were performed in part as previously described using publicly available head and neck squamous cell (HNSC) tumor data from TCGA [23]. Mutation and copy number data were downloaded from cBioPortal for Cancer Genomics site (<http://cbioportal.org>) which enables one to explore, visualize, and analyze multi-dimensional cancer genomics data [24]. RNA-seq and GISTIC copy number data were downloaded from The Broad Institute TCGA GDAC Firehose (gdac.broadinstitute.org), which provides TCGA Level 3 data and Level 4 analyses packaged in a form amenable to immediate algorithmic analysis [5]. Pseudo counts for RNA-seq were generated (RSEM+1) and all data was Log2 transformed. All analyses were performed in R. Copy number analyses were performed using GISTIC2.0 which identifies genomic regions that are significantly gained or lost across a set of tumors [25,26]. The pipeline filtered out normal samples from the segmented copy-number data by inspecting the TCGA barcodes and then executed GISTIC version 2.0.22 (Firehose task version: 140) on 522 HNSCC tumor samples (Broad Institute TCGA Genome Data Analysis Center (2016): SNP6 Copy number analysis (GISTIC2). doi:10.7908/C1V987FP). Each aberration is assigned a G-score that considers the amplitude of the aberration as well as the frequency of its occurrence across samples. False Discovery Rate q-values are then calculated for the aberrant regions, and regions with q-values below a user-defined threshold are considered significant. The Kaplan-Meier (KM) survival analysis was performed using the UCSC Xenabrowser and by extracting cases ($n = 73$) with high (top half) and low (bottom half) of *CRTC1*, *CRTC2*, or *CRTC3* expression in primary tumors with p16 testing from the TCGA HNSCC dataset and using disease specific survival data to generate the KM plot in Prism GraphPad.

Clinical Samples

All research involving human tumor tissues was reviewed and approved by The University of North Carolina at Chapel Hill Institutional Review Board under IRB protocols 15-1604 and 17-2947. Slides used were reviewed for presence of evaluable tumor by a board-certified pathologist.

Cell culture

Immortalized 'Normal' oral keratinocyte (NOK) cell lines OKF4-TERT1, OKF4-E6/E7, OKF6-TERT1, and OKF6-E6/E7 (a gift from Jim Rheinwald and Matthew Ramsey, Harvard University, Boston, MA) were grown in keratinocyte serum free media (KSFM) from (Gibco, cat. #: 17004-042). The OKF6/OKF4 lines were grown in KSFM media supplemented with 25 μ g of bovine pituitary gland extract (BPE) and 0.2 ng/ml of EGF and 0.3 mM of CaCl_2 , and 1x of PSG [27,28]. The HPV-negative cell lines UM-SCC74A, UM-SCC5, UM-SCC11A, and UM-SCC14A (a gift from Thomas Carey, University of Michigan, Ann Arbor, MI) were grown in DMEM (Gibco, cat. #: 11965-092) supplemented with 10% heat-inactivated FBS, 1x PSG, 1x GlutaMAX, and 1x MEM non-essential amino acids (Gibco, cat. #: 11140050). The additional HPV-negative cell lines SCC15 and SCC25 (a gift from Ben Major, UNC-Chapel Hill, Chapel Hill, NC) were grown according to ATCC cell culture conditions. The HPV(+) cells UM-SCC47-C3, 93-VU-147T-C5, UD-SCC2-C6 (SCC2), and UPCI-SCC090-C35, were previously subcloned [29] and cultured in DMEM media supplemented with 10% FBS, 1x PSG, and 1x GlutaMAX.

Generation of MEKK1 knockdown stable cell lines

Lentiviruses (pLKO.1 lentivirus vector) were packaged as previously described [20,30-32]. Briefly, the pLKO.1-Scramble or pLKO.1-MAP3K1 shRNA plasmids (kind gift from Gary Johnson, UNC-Chapel Hill, Chapel Hill, NC) were co-transfected with VSV-G envelope plasmid and d8.2 gag/pol helper plasmids into Lenti X-293T cells (Takara #632180) seeded in 10 cm TC dishes in 7 mL of media. Transfections were performed using 1 mg/mL Polyethyleneimine (PEI) (VWR #BT129700). Briefly, 1.5 μ g VSV-G, 5 μ g d8.2 and 6 μ g of the pLKO.1 constructs were brought to 500 μ L with OptiMEM (LifeTech #1158021) and vortexed briefly. In a separate tube, 25 μ L PEI (2 μ L PEI/ μ g DNA) was added to 475 μ L OptiMEM and vortexed briefly. Both solutions were incubated at room temperature for 5 min, then combined and incubated for an additional 20 min at room temperature. This mixture was then added dropwise to the seeded Lenti X-293T cells. The next day, cell culture media was replaced with DMEM supplemented with 1x NaPyr, 10 mM HEPES, 1X GlutaMAX, and 1X PSG (no FBS). Two days later, media was collected and filtered through a 0.45 μ m PVDF membrane and then viral particles were concentrated via ultracentrifugation (100,000 g for 2 hr at 4°C) into a sucrose cushion. Concentrated virus was resuspended in cold PBS and either stored at -80°C or used immediately for transduction. The HPV-negative UM-SCC74A and the HPV-positive UM-SCC47 cells were then transduced with each lentivirus containing either scramble or one of three different MAP3K1 shRNAs and selected using puromycin for two weeks at a concentration of 0.75 μ g/ml (SCC47) or 2 μ g/ml (SCC74A).

RNA isolation and real-time qPCR

RNA was isolated from HPV-positive and HPV-negative HNSCC cells and oral keratinocyte cells using the NucleoSpin RNA kit (Macherey-Nagel, #740955) in accordance with the manufacturer's protocol. cDNA was made from 0.65 μ g of RNA (HNSCC and NOKs) using the iScript cDNA Synthesis Kit (BioRad #170-8891). Copy number for CRTC1-3, was determined by establishing standard curves with 100 to 1 \times 10⁶ copies of CRTC1-3 cDNA containing expression plasmids. Relative gene expression

of MEKK1, and CRTC2 targets was determined using the 2 ^{$\Delta\Delta\text{Ct}$} method and normalized using human and mouse RPL23. Expression in HNSCC cell lines relative to NOKs was calculated using the ΔCt of OKF6-TERT1. qPCR was performed using FastStart Universal SYBR Green Master Mix (Roche, cat. #04913850001) with 1/40 volume of the cDNA iScript reaction, and 0.25 μ M of primers.

Transfections and adenovirus transductions

Transfections of oral keratinocyte (OKF6-TERT1) and HNSCC (UM-SCC74A, UM-SCC47, 93-VU-147T) cell lines were performed using Lipofectamine 3000 (Life Technologies, cat. #L3000015) per manufacturer's protocol. UM-SCC47 and 93-VU-147T cells were plated at 60% confluency into a 6 well plate, transduced with 50MOI (multiplicity of infection) of CRTC2-RNAi or non-specific-RNAi adenoviruses the following day (kindly provided by Marc Montminy, Salk Institute La Jolle, CA [33]). 24 hours after transduction cells were plated for Luciferase, growth curve, and migration assays.

Plasmid constructs

4x CRE Luciferase (4xCRE-Luc) reporter was made by cloning the cAMP Response Element (CRE) binding sites from the pXP2-Cre-reporter [34] into pGL4.15 (Promega, cat. #E6701) vector using the 5' Kpn I and 3' Sac I restriction sites for cloning purposes. The SRE-Luc construct was purchased from Clontech (cat. #K2049-1). The eGFP construct was purchased from Clontech (cat. #6085-1).

Luciferase reporter assays

OKF6-TERT1, UM-SCC74A, UM-SCC47, 93-VU-147T, and UM-SCC74A/11A/47 stables (scramble-shRNA or MEKK1-shRNA) cell lines were plated into a 24 well plate at 60% confluency. 24 hours later the cells were transfected with 4xCRE-Luc (450ng) plus GFP (50ng) or SRE-Luc (450ng) plus GFP (50ng) plasmids using Lipofectamine 3000 (Life Technologies, cat. #L3000015) per manufacturer's protocol. The following morning the cells were treated with either DMSO (control) or 3-isobutyl-1-methylxanthine (IBMX, 180 μ M) and forskolin (FSK, 10 μ M) to stimulate the cAMP pathway. Four hours later the cells were lysed and fluorescence and luminescence were read using a Cytation5 plater reader (BioTek Instruments, Inc.). GFP fluorescence intensity was used to normalize for differences in transfection efficiency. For cells transduced with adenoviruses containing non-specific or CRTC2 RNAi, cells were transduced in a 6 well plate, and plated into a 24 well plate 24 hours after transduction with adenoviruses. After plating into a 24 well plate, bioluminescent light output of the luciferase reporter was quantified.

Western Blot

OKF6-TERT1, UM-SCC74A, UM-SCC47, 93-VU-147T, and HEK293A (positive control) cells were treated with either DMSO or a combination of IBMX (180 μ M) and FSK (10 μ M) for 30 min at 37°C. Cells were pelleted and whole cell lysates were prepared in lysis buffer containing 250 mM NaCl, 50 mM Tris (pH 7.4), 50 mM NaF, 0.1 mM NaVO_4 , 5 mM EDTA, and 0.1% Triton X-100 supplemented with protease inhibitors (cCompleteTM, EDTA-free Protease Inhibitor Cocktail - Roche, cat. #04693132001) and phosphatase inhibitors (phosphoSTOP, - Roche, cat. #10917400). For examination of CRTC2 localization, UM-SCC74A-scramble-shRNA, UM-SCC74A-MEKK1-shRNA, UM-SCC47-scramble-shRNA, and UM-SCC47-MEKK1-shRNA non-stimulated stable cells were pelleted, and cytosolic and nuclear proteins were extracted using the Ne-Per nuclear and cytosolic extraction kit (Thermo Fisher Scientific, cat.

#78833) following the manufacturer's protocol. Protein concentrations were determined using a bicinchoninic acid (BCA) assay (Thermo Fisher Scientific, cat. #23252). Lysates (20–50 μ g) were loaded onto mini-8% tris-glycine polyacrylamide gels and proteins were separated using sodium dodecyl sulfate-polyacrylamide gel electrophoresis (SDS-PAGE), then transferred to a 0.45 μ m nitrocellulose membrane (GE Healthcare Life Sciences, cat. #10600011) using a Bio-Rad Transblot Turbo System set at 1.0 Amps (constant), 25 volts, and run for 22 mins. Membranes were blocked for 1 hour at room-temperature in TBS-T + 5% milk and then incubated overnight at 4°C with primary antibodies for CRTC2 (1:5000 – Covance, affinity-purified rabbit polyclonal clone #3364), CREB (1:10,000 – Millipore Sigma, cat. #06-863) diluted in TBS-T plus 3% milk. Following primary antibody incubation, membranes were washed and probed with Horseradish peroxidase (HRP)-conjugated goat anti-mouse (1:2500 – Thermo Fisher, cat. #31432) or donkey anti-rabbit (1:2500 to 1:5000 – Thermo Fisher, cat. #31458) secondary antibodies for 1–2 hours at room-temperature. Blots were imaged using Clarity ECL (Bio-Rad, cat. #: 170-5060) and ImageQuant LHS4000 (GE). Data are normalized and cell fractionation confirmed using internal loading controls, anti- α -Tubulin (1:5000 – Sigma Aldrich, cat. #T5168) and anti-CREB for nuclear and cytosolic fractions respectively, or anti- β -actin (1:5000 – Sigma Aldrich, cat. #A3854) for whole cell lysates. Densitometry analysis was performed using ImageQuant TL software (GE).

Immunofluorescence

The OKF6-TERT1, UM-SCC74A, UM-SCC47, and 93-VU-147T cells were plated at approximately 40 – 50% confluency into chamber slides (Nunc™ Lab-Tek™ II, cat. #154526). Cells were treated with either DMSO or IBMX (180 μ M) + FSK (10 μ M) for 30 min. Following treatment, cells were washed with PBS and fixed for 15 min with pre-warmed 4% PFA. Cells were permeabilized using 0.25% Triton X-100 incubation for 10 min. Cells were blocked using 5% BSA in PBS for 1 hour and then stained with anti-CRTC2 antibody (1:500, overnight 4°C – Covance, affinity-purified rabbit polyclonal clone #3364) and anti-rabbit secondary antibody conjugated to Alexa Fluor 594 (1:400 room-temperature 1 hour – Fisher Scientific, cat. #R317117), stained with phalloidin to show cytoskeleton, and mounted using ProLong Gold with Dapi (Invitrogen, cat. #P36966). The cells were examined using an Olympus IX73 microscope with 40X objective and images taken using cellSens software (Olympus).

For MAPK inhibitor-induced CRTC2 cytoplasmic re-localization experiments, 50,000 cells/chamber of UM-SCC47 cells were plated into chamber slides. Cells were then treated with pharmacologic agents targeting the mitogen signaling axis including 10 μ M of the p38 inhibitor - SB, SB203580, 300 nM of the ERK1/2 inhibitor - SCH, SCH772984, or 50 nM of the MEK1/2 inhibitor - GSK, GSK212 for 24 hours. Following treatment, cells were washed with PBS and fixed for 15 min with 4% PFA. Cells stained with anti-CRTC2 antibody (1:500, overnight 4°C), anti-rabbit secondary, phalloidin, DAPI, and mounted as described above. Nuclear versus cytoplasmic CRTC2 was quantified using Cyation5 slide imager. Briefly, a nuclear mask was generated (DAPI) and CRTC2 immunofluorescence intensity was quantified within the nucleus. Next, a whole cell mask was generated (phalloidin) and whole cell CRTC2 immunofluorescence intensity was quantified. Lastly, cytoplasm specific CRTC2 intensities were calculated by subtracting the nuclear CRTC2 fluorescence intensities from the whole cell CRTC2 fluorescence for a given field of view. Data was graphed as nuclear:cytoplasm CRTC2 staining intensities.

Immunohistochemistry (IHC)

Chromogenic immunohistochemistry (IHC) was performed at the UNC Pathology Services Core on paraffin-embedded tissues that were sectioned at

5 micrometers. All IHC was carried out in the Bond III Autostainer (Leica Microsystems Inc.). Slides were dewaxed in Bond Dewax solution (AR9222) and hydrated in Bond Wash solution (AR9590). Antigen retrieval was performed for 20 min at 100°C in Bond-Epitope Retrieval solution 1, pH-6.0 (AR9961). For the CRTC2 antibody (Covance, affinity-purified rabbit polyclonal clone #3364), slides were incubated at a dilution of 1:500 for 1 hr then ImmPress HRP anti-rabbit IgG secondary (Vector Laboratories, cat. # MP-7451). Stained slides were dehydrated and coverslipped with Cytoseal 60 (Thermo Fisher, cat. #8310-4). Positive and negative controls (no primary antibody) were included during staining runs. The slides were digitally scanned at 20X magnification using Aperio AT2 (Aperio Technologies, Vista, CA) and uploaded to the Aperio eSlideManager database (Leica Biosystems Inc) at the Pathology Services Core at UNC.

Digital Imaging and Analysis

Slides DAB stained for CRTC2 were digitally scanned using the Aperio ScanScope-XT (Aperio Technologies; Vista, CA). All images were scanned at an apparent 20x magnification and uploaded to the Aperio eSlideManager database (version 12.4.3, Leica Biosystems; Buffalo Grove, IL) at the Pathology Services Core at UNC. For analysis of CRTC2 subcellular localization, slides stained CRTC2 were digitally segmented into individual cores using TMA Lab (Aperio Technologies; Vista, CA). Whole tissue section images were digitally annotated using Aperio ImageScope to remove staining artifacts and tissue folds before they were analyzed. The Cytoplasmic v2 algorithm (Aperio Technologies) was used to analyze CRTC2 staining. Using this algorithm, cells were analyzed for DAB signal and the number and percentage of cells with light (1+), medium (2+) and strong (3+) cell staining was determined. The average DAB intensities in cells, cytoplasm and nuclei were also determined.

Scratch assay

UM-SCC47 cells transduced with adenoviruses containing either non-specific-shRNA or CRTC2-shRNA were plated into 2 well removable silicone inserts (attached to a 6 well plate) at 100% confluency (Ibidi, cat. #80209) and incubated overnight in low serum media (0.5% FBS). 16–24 hrs later, inserts were removed, cells were washed with PBS, and complete media was added. Images of the cells were taken using an Olympus IX73 microscope with 40X objective and images taken using cellSens software (Olympus) after addition of complete media and every couple of hours to monitor scratch-migration. The scratch area was quantified manually using ImageJ (NIH, Bethesda, <https://imagej.nih.gov/ij/>) and normalized to time zero scratch area.

Invasion assay (Matrigel Coated Transwell)

Cells were reverse-transduced by seeding 400,000 UM-SCC-47 cells in a 6 well plate with adenovirus of interest (Ad-shNS or Ad-shCRTC2) in 1.5 mL complete media. Cells were cultured for 24 hr and were then trypsinized, washed, counted, and resuspended in low-serum media (regular culture media with 0.5% FBS). Prior to seeding cells onto the transwell chamber (Falcon permeable-transwell chambers- 8 μ m pore membrane, cat#: 353097), the transwell membrane was first coated with 5 % Matrigel (Corning, cat#: 356234). Briefly, 100 μ L of 5 % Matrigel solution was added to the transwell chamber, which was then incubated for 1 h in a humidified 37°C, 5% CO₂ cell culture incubator to ensure polymerization. Postpolymerization, the transwell chamber was placed in a 24 well plate well containing 1 mL of complete UM-SCC cell culture media (chemoattractant). Cells were seeded (UM-SCC-47 = 200,000 cells/transwell) into the transwell chamber in 500 μ L of low-serum media and allowed to invade through the Matrigel and onto the bottom side of the transwell membrane for 36 hr. Thirty-six hrs postseeding, cells were fixed using 10% formalin, 15 min at room temperature. Cells were

visualized using 0.05% crystal violet, 60 min incubation at room temperature followed by 5 washes using distilled water. Noninvaded cells still adhered to the 'top-side' of the transwell chamber were removed using cotton swabs. Invaded cells were imaged in brightfield using a Cytation 5 plate imager. Total invaded cell area was quantified using the Analyze Particles function in ImageJ software.

Growth curve assay

UM-SCC47 cells transduced with adenoviruses containing either non-specific-shRNA or *CRTC2*-shRNA were plated into a 48 well plate at a concentration of 10,000 cells per well. Twenty-four hours after plating, cells were washed with PBS to remove non-adherent cells and fresh media was added to each well. Cells were imaged every 2 hours using a 10x objective and percent confluency was calculated by IncuCyte ZOOM (Essen Biosciences) using default cell area confluency masking.

Statistical Analyses

Statistical analyses were performed with GraphPad Prism (version 9) using Student's *t*-test, one-way ANOVA or 2-way ANOVA where applicable. Data are presented as mean \pm SD or mean \pm SEM as indicated in the figure legends.

Results

CRTC2 activation in HNSCC is associated with poor patient outcomes

To begin investigating the mechanisms involved in cAMP/CREB pathway activation in HNSCC, we sought to determine whether this activation results from the genomic alteration of its upstream regulators. To this end, we analyzed the PanCancer dataset from TCGA to identify the frequency of *SKT11* and *CRTC* family alterations. In contrast to lung adenocarcinomas (LUAD) which frequently harbor inactivating mutations in *SKT11*, the critical upstream negative regulator of CRTCs, [35,36], few *SKT11* inactivating mutations or deletions are present in HNSCCs (Fig. 1A). Alternatively, amplification of *CRTC* family members can also lead to increased CREB activity. Thus, we next looked at the frequency of *CRTC1*, *CRTC2* and *CRTC3* amplification across the TCGA PanCancer dataset and found that *CRTC2* is the most amplified family member in tumors at 4% (compared to 1.9% for both *CRTC1* and *CRTC3*) (Supplementary Figure S1A). However, when we broke the PanCancer dataset down by tumor type, we again observed that *CRTC2* was rarely amplified in HNSCCs similar to *SKT11* (Fig. 1B and Supplementary Figure S1B).

In the absence of either loss of the *SKT11* negative regulator or amplification of the *CRTC2* gene locus, we next wanted to determine if any *CRTC* family member is over expressed in HNSCCs as compared to normal. Indeed, *CRTC2*, but not *CRTC1* or *CRTC3*, is significantly increased ($p = 1.7\text{e-}10$) expression compared to tumor adjacent normal (Fig. 1C). To place this in the context of other tumor types, we compared the cohort level expression of HNSCCs from TCGA against those tumor types with most frequent *SKT11* loss and thus *CRTC*/CREB activation. While HNSCCs expressed *CRTC2* at a lower level than UCEC or LUAD, its expression was greater than tumors from ESCA and STAD, placing well within the range of expression of tumors associated with aberrant CREB activity (Fig. 1D). As aberrant CREB activity has been previously associated with tumor stage, grade, metastasis, and worse prognosis [37–39], we then evaluated if increased expression of *CRTC2* is associated with disease free survival. In primary HNSCC tumors, *CRTC2* expression was associated with a significant decrease ($p = 0.044$) in disease specific survival compared to *CRTC1* and *CRTC3* (Fig. 1E) and trends similarly for progression free survival (Supplemental Figure S1C). Interestingly, *CRTC2* levels are significantly elevated in both

HPV(+) and HPV(-) HNSCCs and increase with stage (Supplementary Figure S1D). These observations suggest that aberrant *CRTC2* regulation may confer poor prognosis in a subset of HNSCC tumors.

CRTC2 is constitutively localized to the nucleus in HNSCC

To investigate the effects of *CRTC2* in HNSCCs, we first set to confirm expression of each *CRTC* family member using a panel of ten independent HNSCC cell lines derived from oral and oropharyngeal sites of different patients and representative of both HPV(+) and HPV(-) HNSCC subtypes. Similar to primary HNSCC tumors, we found *CRTC2* to be the predominantly expressed *CRTC* family member in these HNSCC cell lines (Fig. 2A and Supplementary Figure S2A). Transcriptional co-activator activity of *CRTC* family members is mechanistically regulated in part by phosphorylation and subcellular localization. Under resting conditions, canonically phosphorylated CRTCs are inactive and retained in the cytoplasm, but addition of the adenylyl cyclase agonist forskolin (FSK) to activate cAMP signaling promotes *CRTC* de-phosphorylation and shuttling to the nucleus (Supplementary Figure S2B). Similarly, elevated *CRTC* expression levels can lead to a regulatory imbalance and an increase in hypo-phosphorylated, nuclear CRTCs. However, upon further characterization, four independent normal (nontransformed, immortalized oral keratinocytes) control cell lines displayed a similar phosphorylation pattern as all ten HNSCC cell lines examined such that phosphorylated *CRTC2*, which is predicted to correspond with a transcriptionally inactive form of *CRTC2*, is the predominant *CRTC2* species observed (Fig. 2B).

To examine the impact of *CRTC2* phosphorylation status on the transcriptional regulation of CREB target genes, cells were transfected with a cAMP-responsive luciferase reporter and treated with FSK and the phosphodiesterase inhibitor 3-isobutyl-1-methylxanthine (IBMX) to activate and increase levels of available cAMP, respectively. While control OKF6-TERT cells displayed robust and significant ($p < 0.001$) increases in reporter activity, HNSCC cells displayed high basal levels of reporter activation and stimulation of cAMP signaling did not further induce reporter activity (Fig. 2C and Supplementary Figure S2C). These findings suggest that *CRTC2* may already be active at basal states despite its phosphorylated state. Surprisingly, despite robust levels of *CRTC2* phosphorylation observed in HNSCC cell lines (Fig. 2B), immunofluorescence (IF) staining in basal, non-stimulated HNSCC cells revealed constitutive nuclear compartmentalization compared to normal oral keratinocytes which only undergo shuttling of *CRTC2* to the nucleus upon FSK/IBMX stimulation state (Fig. 2D and Supplementary Figure S2D).

We next sought to extend these findings based on HNSCC cell lines to a cohort of primary human HNSCC tumors with available clinical information regarding HPV status from the surgical pathology department at the University of North Carolina (UNC) Hospitals (Chapel Hill, NC) (Table 1). We performed immunohistochemistry (IHC) on formalin fixed paraffin embedded (FFPE) sections of these tumors (Fig. 3A). Consistent with our *in vitro* results in HNSCC cell lines (Fig. 2D), we found that staining for *CRTC2* protein was significantly higher ($p < 0.01$) in the nucleus of primary HNSCC tumors compared to the cytoplasm (Fig. 3B). Moreover, a significant increase ($p < 0.05$) in nuclear localization was observed in HNSCC tumors where HPV status was confirmed by p16 IHC and HPV *in situ* hybridization (ISH) assays (Fig. 3C). These data suggest that in human HNSCC tumors, upstream signaling cascades promote nuclear shuttling and constitutive activation of *CRTC2* irrespective of HPV status.

MEKK1 controls *CRTC2* nuclear translocation and transcriptional activation

Aberrant *CRTC* activation is commonly associated with a loss of LKB1 activity in cancers [16,17,40]. However, our bioinformatic analysis of

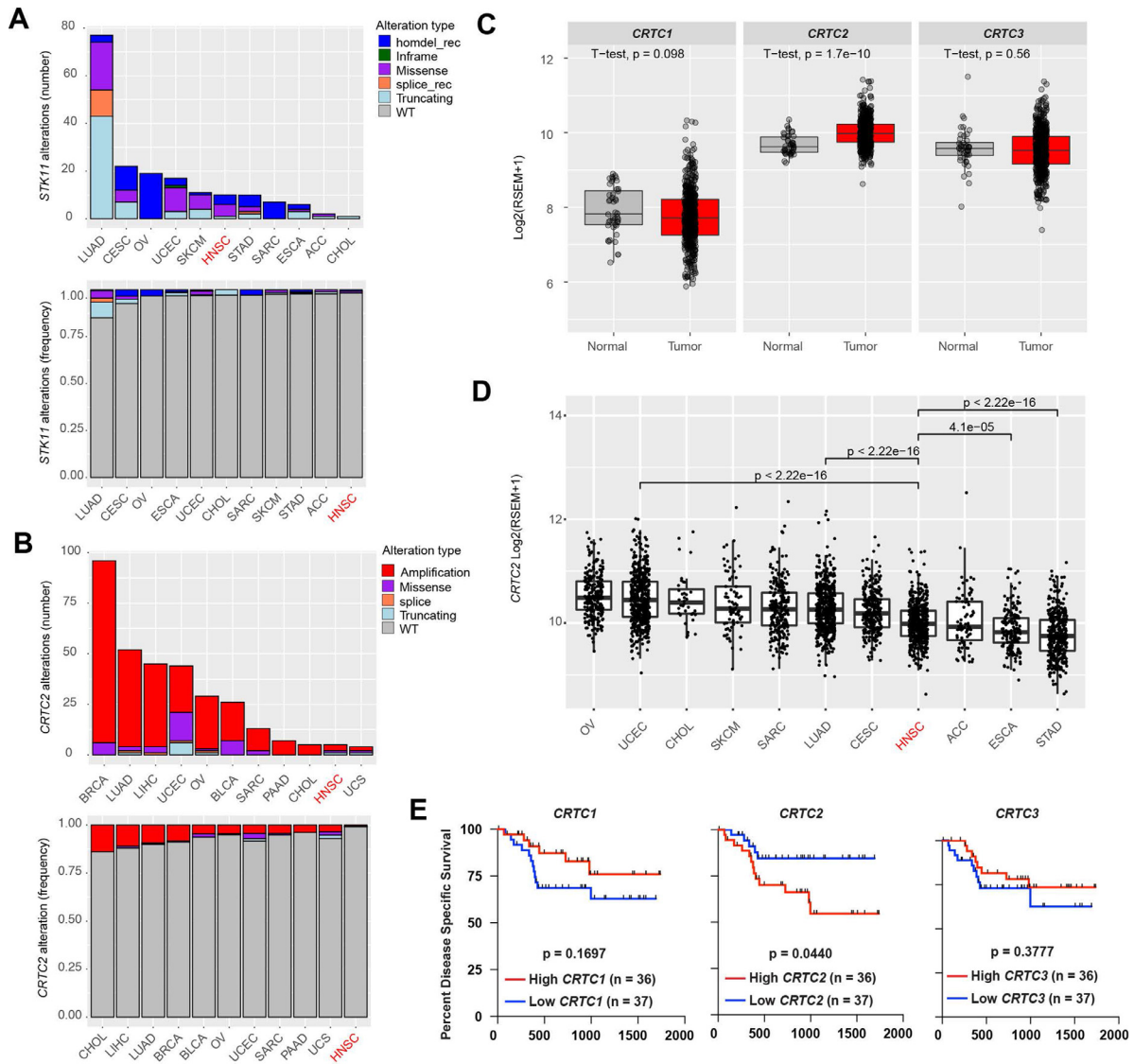


Fig. 1. Association of *CRTC2* expression in head and neck squamous cell carcinoma (HNSCC) with patient survival. **(A)** PanCancer analysis of TCGA tumor types is shown with the total number (*top*) or frequency (*bottom*) of *STK11* deletion or mutation plotted. Comparison of the top 10 tumors of similar tissue type (e.g. mucosal/epithelial) revealed that HNSCCs have the lowest frequency of alteration. LUAD = lung adenocarcinoma, CESC = cervical squamous cell carcinoma, OV = ovarian carcinoma, UCEC = uterine corpus endometrial carcinoma, skcm = skin cutaneous melanoma, HNSC = head and neck squamous cell carcinoma, STAD = stomach carcinoma, SARC = sarcoma, ESCA = esophageal squamous cell carcinoma, ACC = adrenocortical carcinoma, CHOL = cholangiocarcinoma. **(B)** PanCancer analysis of TCGA tumor types is shown with the total number (*top*) or frequency (*bottom*) of *CRTC2* amplification or mutation plotted. Comparison of the top 10 tumors of similar tissue type (e.g. mucosal/epithelial) revealed that HNSCCs have the lowest frequency of alteration. **(C)** Comparison of *CRTC1*, *CRTC2*, and *CRTC3* expression levels in HNSCC tumors relative to normal tissue reveals that *CRTC2* is the only significantly elevated family member ($p = 1.7e-10$). Data were extracted from the TCGA HNSCC RNA-seq dataset and log₂ median-centered expression are plotted ($n = 496$ tumor samples). **(D)** PanCancer comparison of *CRTC2* expression levels in HNSCC tumors relative to tumors of similar tissue type (e.g. mucosal/epithelial). **(E)** Kaplan-Meier (KM) plots of Disease Specific Survival estimated for HNSCC cases with *CRTC1-3* upregulation. Primary tumor samples from the TCGA head and neck cancer dataset were analyzed using the UCSC Xena Functional Genomics Explorer to generate KM plots based on binary high versus low of *CRTC1-3* expression ($n = 74$ tumor samples).

HNSCC TCGA data revealed that loss or mutation in *STK11/LKB1* is uncommon (Fig. 1A). Thus, we next sought to understand what other mechanisms could lead to the observed nuclear localization and activation of *CRTC2* in HNSCC cell lines and tumors. Previous studies by Siu Y-T et al. revealed that non-canonical *CRTC1* phosphorylation induced by MEK1 (or MAP3K1) can promote the nuclear localization and transcriptional activation of *CRTC1:CREB* target genes [22]. Moreover, MEK1 overexpression and/or activation due to aberrant mitogen signaling

has been observed in some HNSCCs [41] making it a candidate for further investigation of its effects on *CRTC2* function.

Analysis of MEK1 expression levels by qPCR showed that MEK1 is not overexpressed in the HPV(-) UM-SCC-74A nor the HPV(+) UM-SCC-47 cell lines compared to normal oral keratinocytes (Fig. 4A). To investigate if MEK1 signaling is aberrantly active and responsible for inducing translocation and activation of *CRTC2*, we depleted MEK1 by short hairpin RNA (shRNA)-mediated knockdown in both UM-SCC-

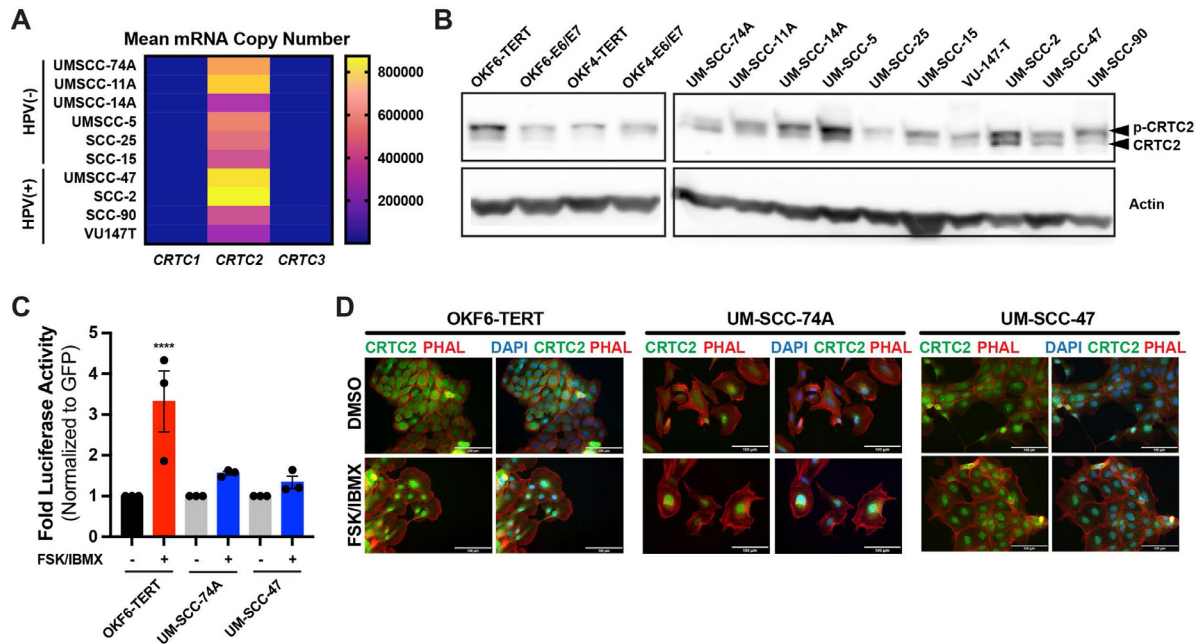


Fig. 2. Constitutive subcellular localization and coactivator activity of CRTC2 within the nucleus of HNSCC cell lines. **(A)** Heatmap of *CRTC1*, *CRTC2*, and *CRTC3* mRNA copy number in various HNSCC cell lines based on HPV status. Quantitative real-time PCR analysis of *CRTC1-3* copy number per 10 ng input RNA calculated based on a standard curve. Cell lines are listed along the y axis with HPV status indicated, and each CRTC family member indicated along the x axis. Data are presented as the mean copy number ($n = 3$ biologic replicates, 4 technical replicates each). **(B)** Western blot showing expression of total and phosphorylated CRTC2 protein in normal oral keratinocytes (OKF lines) compared to HNSCC cell lines. This blot is representative of independent biologic replicates. **(C)** Luciferase reporter assay measuring relative fold induction of a 4xCRE promoter in normal oral keratinocyte cells (OKF6-TERT) versus HPV(-) UM-SCC-74A or HPV(+) UM-SCC-47 cells treated with either vehicle (DMSO) or forskolin (FSK) and IBMX. Co-transfection with a GFP reporter was used for normalization of transfection efficiencies and protein expression. Data are presented as the mean \pm SEM ($n = 3$ biologic replicates, 4 technical replicates each; Student's t test; $***p < 0.001$). **(D)** Representative immunofluorescence images of normal oral keratinocyte cells (OKF6-TERT) versus HPV(-) UM-SCC-74A or HPV(+) UM-SCC-47 cells treated with either vehicle (DMSO) or forskolin and IBMX. Cells were stained with hCRTC2 antibody (green), phalloidin (red), and 4',6-diamidino-2-phenylindole (DAPI; blue). Bar, 100 μ M.

Table 1

Patient characteristics.

Anatomic Site	p16 IHC	HPV high risk strains	ISH	Race	Ethnicity	Sex	Age at onset
Oral Cavity - Floor of Mouth	negative	negative		White	Non-Hispanic	Male	54
Oral Cavity - Oral Tongue (Anterior 2	negative	negative		White	Non-Hispanic	Male	67
Oral Cavity - Oral Tongue (Anterior 2	negative	negative		White	Non-Hispanic	Male	87
Oral Cavity - Oral Tongue (Anterior 2	negative	negative		Black or African American	Non-Hispanic	Female	66
Larynx - NOS ^a	positive	negative		Black or African American	Non-Hispanic	Male	60
Larynx - Supraglottis - NOS	positive	negative		White	Non-Hispanic	Male	58
Oral Cavity - Floor of Mouth	positive	negative		White	Non-Hispanic	Male	50
Oral Cavity - Oral Tongue (Anterior 2	positive	positive		White	Non-Hispanic	Male	44
Oral Cavity - Oral Tongue (Anterior 2	positive	positive		White	Non-Hispanic	Male	57
Oropharynx - NOS	positive	positive		White	Non-Hispanic	Male	63
Oropharynx - Tonsil	positive	positive		White	Non-Hispanic	Male	66

^a NOS - Not otherwise specified

74A and UM-SCC-47 cell lines (Fig. 4B). Effects of MEKK1 knockdown were functionally validated using an AP-1 luciferase reporter and confirmed significant decreases in transcriptional activity in both cell lines (Fig. 4C). Interestingly, MEKK1 knockdown only reduced CRTC2:CREB activity (40% decrease, $p < 0.05$) in HPV(+) UM-SCC-47 cells, but not in HPV(-) UM-SCC-74A or UM-SCC-11A cell lines (Fig. 4D and Supplementary Figure S3). Notably, MEKK1 knockdown was also associated with a significant increase ($p < 0.01$) in the redistribution of CRTC2 from the nucleus to the cytoplasm (Fig. 5A and Supplementary Figure

S4A). Treatment of UM-SCC-47 cells with inhibitors that target known downstream effectors of MEKK1 signaling (e.g., p38, ERK1/2, MEK1/2) showed that only SB203580, an inhibitor of the known MEKK1 effector p38, resulted in a significant and robust decrease in CRTC2 nuclear localization (Fig. 5B). There was a trend toward decreasing CRTC2 nuclear localization using the ERK1/2 inhibitor SCH772984, however the difference was not statistically significant. These data suggest that a MEKK1-p38 signaling axis, which is known to be a critical oncogenic signaling pathway, mediates the activation and localization of CRTC2 in HPV(+) HNSCC.

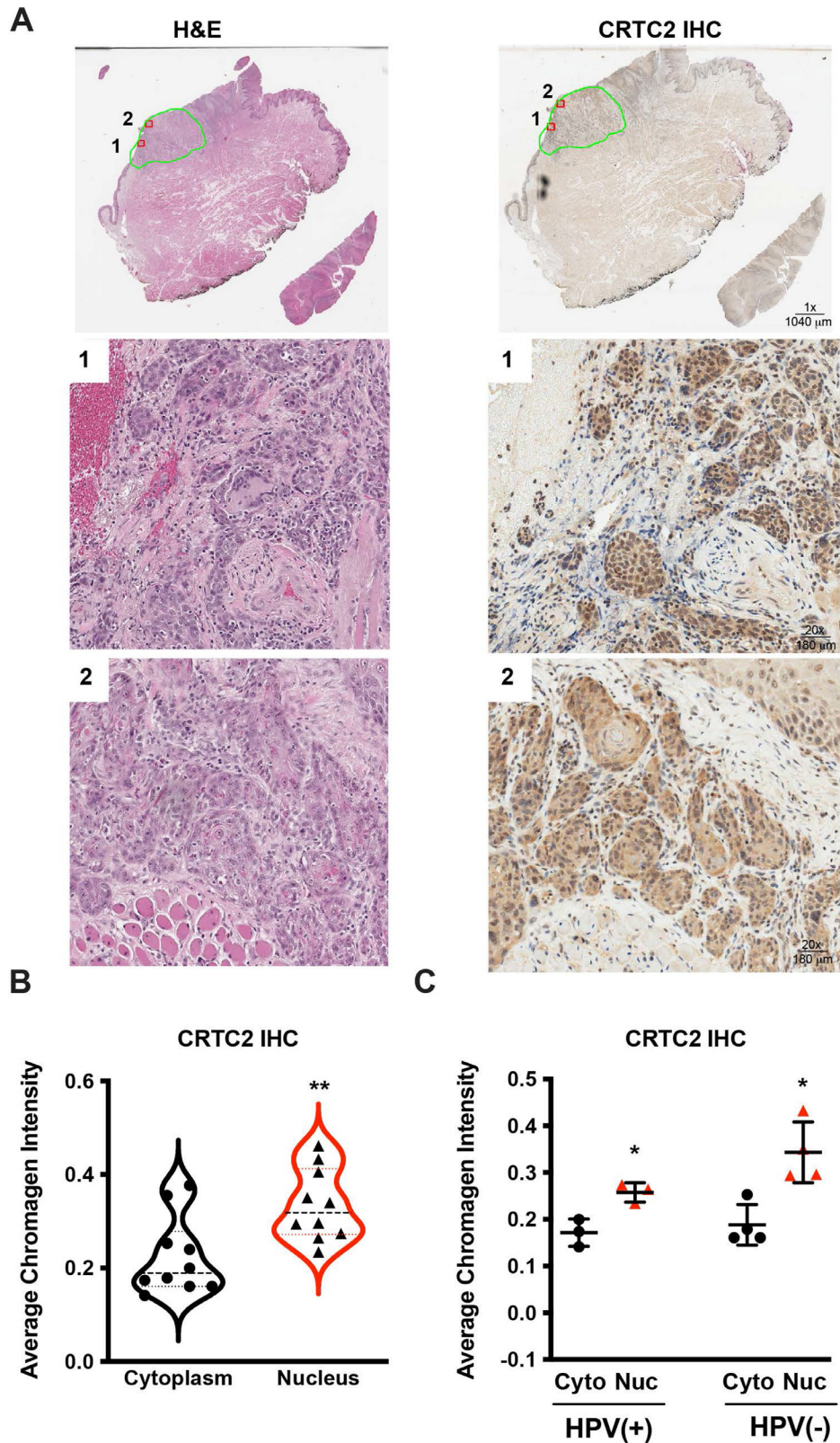


Fig. 3. CRTC2 immunostaining reveals nuclear subcellular localization in HNSCC tumors. (A) Representative immunohistochemical analysis of formalin fixed paraffin embedded sections of HNSCC tumors stained with anti-CRTC2. Magnification, 1x; bar, 1040 μ m or inset image 20x; bar, 180 μ m. (B) Aperio digital quantification of CRTC2 IHC staining in the cytoplasmic versus nuclear subcellular compartments in primary tumor tissue samples of HNSCCs. Data are presented as the mean \pm SEM ($n = 10$; Student's t test; ** $p < 0.01$). (C) Aperio digital quantification of CRTC2 IHC staining in the cytoplasmic versus nuclear subcellular compartments of primary tumor tissue samples from HPV-verified HNSCC tumors based on p16 IHC and HPV ISH status. Data are presented as the mean \pm SEM ($n = 7$; Student's t test; * $p < 0.05$).

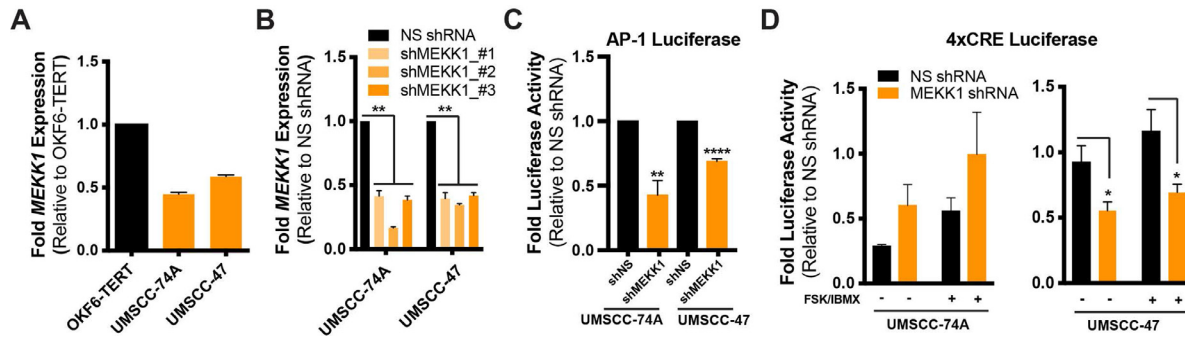


Fig. 4. MEK1 signaling regulates CRTC:CREB-responsive promoter activity in HPV(+) HNSCC cells. **(A)** Quantitative real-time PCR analysis of relative *MEK1* expression levels in HNSCC cells compared to normal oral keratinocytes. Data are presented as the mean \pm SEM ($n = 3$ biologic replicates, 4 technical replicates each). **(B)** Quantitative real-time PCR analysis demonstrating knockdown of *MEK1* using three separate MEK1-targeted shRNAs (#1, #2, and #3) relative to a control shRNA (shNS). Data are presented as the mean \pm SEM ($n = 3$ biologic replicates, 4 technical replicates each; Student's t test; $**p < 0.01$). **(C)** Luciferase reporter assay measuring relative fold induction of a MEK1:AP-1 responsive promoter in HPV(-) UM-SCC-74A or HPV(+)-UM-SCC-47 cells stably transduced with either shNS or shMEK1 shRNAs. Data are presented as the mean \pm SEM ($n = 3$ biologic replicates, 4 technical replicates each; Student's t test; $**p < 0.01$, $****p < 0.0001$). **(D)** Luciferase reporter assay measuring relative fold induction of a 4xCRE CRTC:CREB-responsive promoter in HPV(-) UM-SCC-74A or HPV(+)-UM-SCC-47 cells stably transduced with either shNS or shMEK1 shRNAs and treated with either vehicle (DMSO) or forskolin (FSK) and IBMX. Data are presented as the mean \pm SEM ($n = 3$ biologic replicates, 4 technical replicates each; Student's t test; $*p < 0.05$).

CRTC2 activity is an important regulator of oncogenic functions in HPV(+) HNSCC

To determine the effects of aberrant CRTC2 activation and nuclear localization on downstream tumor promoting processes in HPV(+) HNSCC, we functionally disrupted CRTC2:CREB transcriptional activity via shRNA-mediated knockdown of CRTC2 (Fig. 5C and Supplementary Figure S4B). Live-cell, kinetic proliferation assays revealed that non-treated wild-type UM-SCC-47 cells and cells transduced with scrambled non-specific shRNA adenovirus reach 50% confluency after 36 h ($GC_{50} = \sim 42$ h), but CRTC2 knockdown significantly slows proliferation and increases this time to confluency more than double ($GC_{50} = \sim 90$ h, $p < 0.001$) relative to control (Fig. 5D). Since aberrant CRTC1 activity has been correlated with aggressive tumor behavior [42–44] and we see decreased DSS in patients with high CRTC2, we next examined the association between CRTC2 and cell behavior. Analysis of 2D cell migration in scratch assays confirmed that adenoviral shRNA-mediated knockdown of CRTC2 at two different multiplicities of infection (MOI) correlates with significantly reduced rates of scratch closure ($\sim 75\%$ decrease, $p < 0.001$) compared to control UM-SCC-47 cells (Fig. 5E-F). Moreover, reduced levels of CRTC2 also correlated with a dramatic decrease in 3D cell invasion through Matrigel in transwell assays for UM-SCC-47 cells (Fig. 5F). These findings were validated using an independent HPV(+) cell line, VU-147-T (Supplementary Figure S4C-D). Collectively, our findings indicate that the CRTC2:CREB pathway is constitutively active in HNSCC, and this activation is mediated by MEK1-p38 signaling, which promotes oncogenic properties in HPV(+) cells.

Discussion

The transcription factor CREB is overexpressed or hyperactivated in different cancers and its overexpression has been correlated with patient survival, metastasis, and therapeutic response [8,10,14]. Analysis of mRNA and protein expression patterns in human breast cancer showed that patients with metastasis and a poor prognosis had increased levels of CREB1 accompanied by reduced disease-free survival [45]. Similarly, patients with acute leukemia whose bone marrow over-expressed CREB had an increased risk of relapse and decreased event-free survival [46]. Furthermore, work

by Johannessen et al. suggests that reactivation of CREB via PKA in melanoma tumors promotes resistance to RAF-MEK inhibition [47]. The activation of CREB can occur via phosphorylation of residues in the kinase inducible domain (KID) by several kinases including AKT, ERK1/2, p90RSK, protein kinase A, p38, and calcium/calmodulin-dependent kinases [15,48–50]. However, transcriptional activity of CREB is not only regulated by phosphorylation but also by the activation status family of the CRTC coactivators [15,51].

Our findings corroborate previous studies indicating a role for CRTC2 in cancer [52] and mechanistically reveal that constitutively active CRTC2 is localized in the nucleus and associated with poor patient prognosis in HNSCCs. Knockdown of MEK1 in HPV(+), but not HPV(-), HNSCC cells promoted shuttling and re-localization of CRTC2 to the cytoplasm thereby resulting in decreased nuclear CRTC2/CREB transcriptional activity. Further, experiments using inhibitors that target known effectors downstream of MEK1 identified p38 as a candidate responsible for mediating the regulation of CRTC2 nuclear localization and activity. Lastly, knockdown of CRTC2 inhibited proliferation, 2D migration, and also 3D invasion of HPV(+) HNSCC cells. Although the role of CRTC and CREB in cancers can vary (i.e., oncogenic versus tumor suppressive), our data indicate that the CRTC2/CREB pathway has a pro-tumorigenic effect on HNSCCs [9,10].

The role of CRTCs in tumorigenesis is still being elucidated and will aid in fully defining the role of CREB in cancer progression. Examples of cancers with known aberrant CRTC activity include salivary MEC, non-small cell lung carcinoma (NSCLC), colorectal carcinoma (CRC), and esophageal squamous cell carcinoma, however, activation of CRTC in these cancers varies [9]. We have previously summarized the frequencies, distribution of somatic mutations, gene fusions, amplifications, deletions, and mRNA expression in CRTC1-3 along with the mechanisms that regulate CRTC activation [9]. Briefly, in non-small cell lung cancers with mutationally inactivated LKB1, CRTC2 is unphosphorylated and constitutively activated due to the loss of LKB1 mediated activation of SIK kinases [17,52,53]. Moreover, like our findings in HNSCC, CRTC2 is associated with poor patient prognosis and is the most frequently expressed CRTC family member in NSCLC.

Mechanistically, the phosphorylation of CRTC2 at Ser171, Ser275, or Ser307 is associated with 14-3-3 binding and localization in the cytoplasm [9,15,33,54]. Upon signal-induced activation, CRTCs undergo translocation

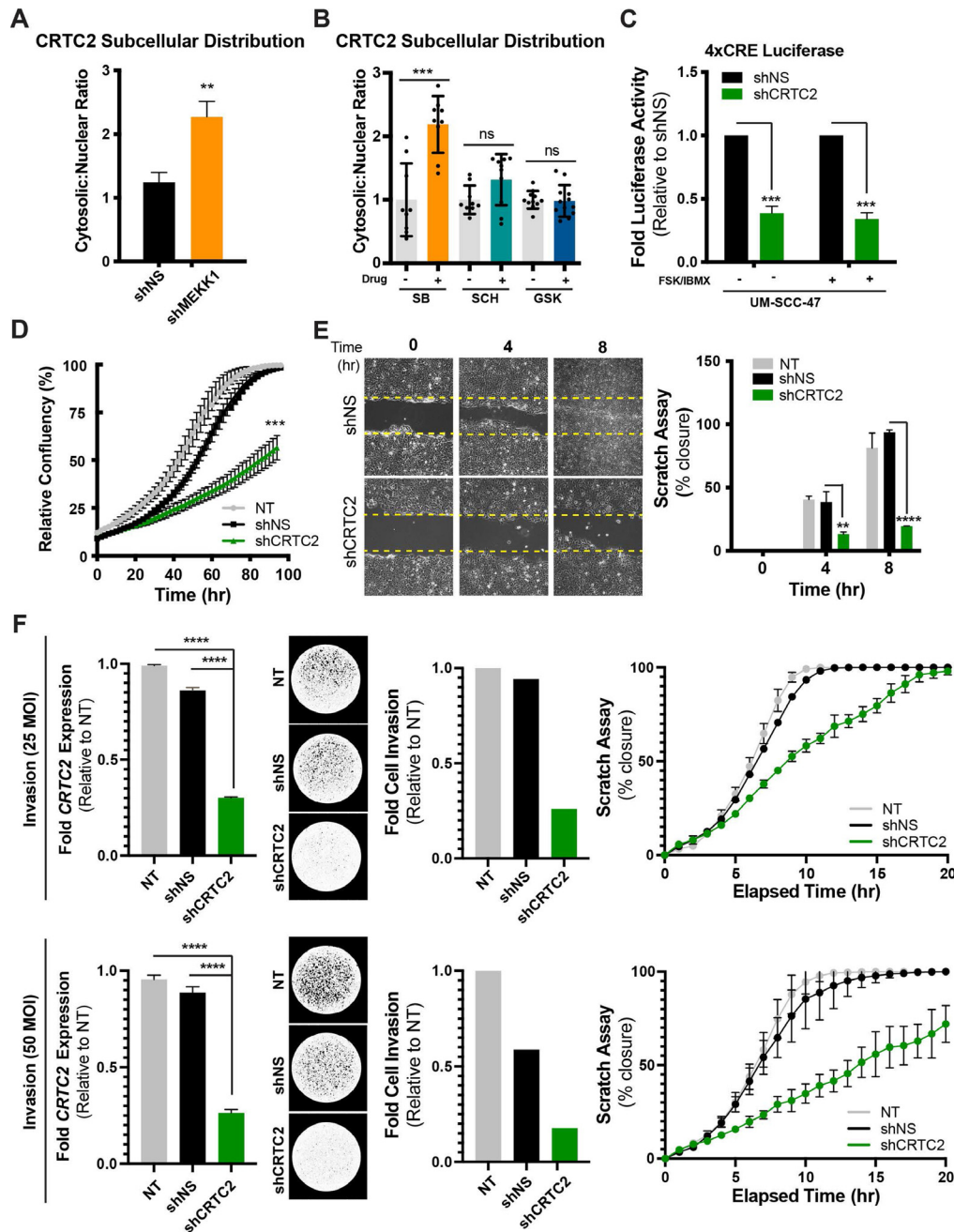


Fig. 5. MEKK1-regulates CRTC2 activity which promotes oncogenic functions in HPV(+) HNSCC cells. **(A)** Quantification of the cytosolic versus nuclear distribution of CRTC2 in HPV(+) UM-SCC-47 cells stably transduced with either shNS or shMEKK1 shRNAs. Data are presented as the mean \pm SEM ($n = 3$ biologic replicates, 10 FOV each; Student's t test; $**p < 0.01$). **(B)** Quantification of CRTC2 subcellular localization in HPV(+) UM-SCC-47 cells treated with pharmacologic agents targeting the mitogen signaling axis (p38i - SB, SB203580; ERK1/2i - SCH, SCH772984; MEK1/2i - GSK, GSK212). Data are presented as the mean \pm SEM ($n = 3$ biologic replicates, 10 FOV each; Student's t test; $***p < 0.001$). **(C)** Luciferase reporter assay measuring relative fold induction of a 4xCRE CRTC:CREB-responsive promoter in HPV(+) UM-SCC-47 cells transduced with adenovirus expressing either shNS or shCRTC2 shRNAs and treated with either vehicle (DMSO) or forskolin (FSK) and IBMX. Data are presented as the mean \pm SEM ($n = 3$ biologic replicates, 4 technical replicates each; Student's t test; $***p < 0.001$). **(D)** Cell proliferation assays showing relative confluency of HPV(+) UM-SCC-47 cells transduced with adenovirus expressing either shNS or shCRTC2 shRNAs. The experiment was performed in biologic triplicate ($n = 4$ technical replicates per experiment) with one representative experiment shown (mean \pm SEM; Benjamini-Hochberg pairwise comparisons; $***p < 0.001$). Data were collected using an IncuCyte live-cell imager; see methods for details. **(E)** Scratch assays performed with HPV(+) UM-SCC-47 cells transduced with adenovirus expressing either shNS or shCRTC2 shRNAs. Images were captured every hour for 24 h to quantify rates of scratch closure. Data are presented as the mean \pm SEM ($n = 3$ biological replicates, with 3 independent FOV per replicate; Student's t test; $**p < 0.01$, $****p < 0.0001$). **(F)** Transwell invasion assays performed with HPV(+) UM-SCC-47 cells transduced with adenovirus expressing either shNS or shCRTC2 shRNAs and using Boyden chambers precoated with Matrigel. After 24 h, cells were stained with 0.05% crystal violet and DAPI, imaged, and counted to quantify rates of invasion. Representative data of independent biologic replicates with adenovirus at two different MOIs are presented as the mean \pm SD (>5 independent FOV were quantified per biologic replicate).

to the nucleus where they bind to the bZIP domain on CREB and initiate transcription of CREB target genes [15]. Canonically, cAMP signaling, along with calcium signaling within excitable cells, induces dephosphorylation and activation of CRTCs [15]. However, recent reports have identified non-canonical mechanisms that lead to the phosphorylation and activation of CRTC1, CRTC2, and CRTC3. For example, MEKK1 mediated phosphorylation within the C-terminal activation domain of CRTC1 can induce its nuclear localization and activation [22]. Similarly, ERK- and CDK-mediated phosphorylation of CRTC3 at S391 leads to recruitment of PP2A, which de-phosphorylates 14-3-3 binding sites and promotes nuclear translocation leading to CRTC3/CREB activation [21]. Interestingly, ERK2 mediated phosphorylation at Ser238 was recently shown to also induce activation of CRTC2 [55], but we did not see a significant decrease in nuclear CRTC2 localization following treatment with the ERK1/2 inhibitor SCH772984 suggesting that phosphorylation of Ser238 or other regulatory motifs via alternate MEKK1 pathways leads to recruitment of phosphatases that remove the inhibitory Ser171 phosphorylation, similar to what was seen in these previous studies with CRTC3 [21,55].

While disrupting ERK signaling did not affect CRTC activity, we did observe a dramatic decrease in CRTC2 nuclear localization following treatment with the p38 inhibitor SB203580. Previous studies showed that increased phospho-p38 expression is present in 79% of HNSCC tissues and that inhibition of p38 decreased tumor growth in xenograft models [56]. Importantly, p38 and MK2 activation during epithelial differentiation are key regulators of the HPV life cycle and are needed for amplification of the HPV genome [57]. However other work on CRTC1 found that overexpressing p38, ERK2, or JNK does not alter CRTC1 transcriptional activity suggesting that the mechanisms regulating subcellular localization and activity of each specific CRTC family member varies depending on context [22]. Possible explanations for these observed differences include 1) the impact of pharmacologic inhibition versus overexpression of downstream MEKK1 effectors, 2) differences in the effects of MEKK1-mediated phosphorylation on other regulatory post-translational modifications, or 3) potential effects of SB203580 on AKT2 inhibition and CRTC regulation [58]. In fact, knockdown of AKT2 and ERK2 significantly decreased phosphorylation of Ser238 on CRTC2 [55], however the authors hypothesized that the impact of AKT2 was due to decreased CRTC2 protein expression rather than an effect on its subcellular localization. Thus, future studies aimed at determining whether AKT2 contributes to CRTC2 activation are merited.

Regarding posttranslational modifications, acetylation, ubiquitination, and glycosylation are each also known to regulate CRTC activity [9,15]. For example, O-glycosylation of CRTC2 at Ser171 blocked phosphorylation of this inhibitory site and increased CRTC2 activity [59]. However, this study did not investigate any potential sites phosphorylated by MEKK1/p38 that may cooperate with O-glycosylation of CRTC2 at Ser171 to promote nuclear localization of CRTC2. Regardless, it is interesting that MEKK1 knockdown impacted the translocation of CRTC2 in the HPV(+) but not the HPV(-) HNSCC cell lines. LKB1 loss is associated with HPV(+) cervical cancers and expression of LKB1 in HPV transformed cells inhibited anchorage independent cell growth, glucose metabolism and invasion and metastasis [60]. The HPV16 E6 oncoprotein was shown to inhibit LKB1 mRNA and protein expression suggesting a possible relationship between HPV and dysregulation of the LKB1/CRTC/CREB signaling axis [61–63]. The influence of HPV infection on LKB1 and the cellular microenvironment could lead to MEKK1-mediated activation of CRTC2. Further experiments are needed to determine if the HPV oncogenes directly impact CRTC2 localization, and thus CRTC2/CREB target gene activation, in HPV(+) HNSCC.

Conclusions

The present study provides important insights into the role that aberrant CREB and CRTC2 activation have on proliferation, migration, and invasion

of cancer cells. Several studies have suggested that increased CREB activity is associated with poor prognosis of several cancers [8,10], but we demonstrate here that knockdown of CRTC2 alone is sufficient to blunt migration and invasion in HPV(+) HNSCC. Thus, our findings have clear translational implications since strategies to inhibit CRTC2 may have therapeutic potential in these HNSCC patients. Collectively, our findings, and that of others, supports a role for aberrant CRTC2/CREB signaling in promoting tumor progression. Additional studies are needed to identify the downstream targets of the MEKK1/p38/CRTC2 circuit in HPV(+) HNSCCs responsible for mediating the proliferative and migration effects observed. However, given the relevance of our findings to HNSCC patient outcomes, further investigation within independent HNSCC model systems such as HPV(+) genetically engineered mouse models (GEMMs) is warranted [64].

Supplementary Material

Supplementary Figure S1. Association of genomic alterations with *CRTC2* expression in cancer. **(A)** cBioportal OncoPrint of CREB coactivator family members for tumors ($n = 10,967$) within the TCGA PanCancer Atlas studies (The Cancer Genome Atlas [TCGA], cBio Cancer Genomics Portal). The types of genomic alterations present in *CRTC1*, *CRTC2*, and *CRTC3* are as labeled in the color legend. **(B)** Copy number landscape derived from FireBrowse for HNSCC (TCGA, Cancer Program Resource Gateway). Red peaks reflect genomic positions of amplified regions and blue peaks reflect genomic positions of deleted regions with the X-axis representing the normalized amplification signals (top) and significance by q value (bottom). The green line represents the significance cutoff at q value = 0.25 ($n = 522$ tumor samples). **(C)** Kaplan-Meier (KM) plots of Progression Free Survival estimated for HNSCC cases with *CRTC2* upregulation. Primary tumor samples from the TCGA head and neck cancer dataset were analyzed using the UCSC Xena Functional Genomics Explorer to generate KM plots based on binary high versus low of *CRTC2* expression ($n = 74$ tumor samples). **(D)** *Left*, comparison of *CRTC2* expression according to HNSCC tumors based on HPV status relative to normal. *Right*, comparison of *CRTC2* expression in HPV positive HNSCC tumors relative to tumor stage of HPV negative HNSCCs. Data were extracted from the TCGA HNSCC RNAseq dataset and log₂ median-centered expression plotted according to the American Joint Committee on Cancer Tumor Stage designations.

Supplementary Figure S2. Characterization of *CRTC2* expression and activity in cell lines. **(A)** Quantitative real-time PCR analysis of *CRTC1-3* copy number per 10 ng input RNA calculated based on a standard curve. Data are presented as mean \pm SEM ($n = 3$ biologic replicates, 4 technical replicates each). **(B)** Western blot showing expression of total and phosphorylated CRTC2 protein from cytoplasmic and nuclear extracts of HEK293T cells treated with either vehicle (DMSO) or forskolin (FSK). This blot is representative of independent biologic replicates. **(C)** Luciferase reporter assay measuring relative total light units from an inducible 4xCRE CRTC:CREB-responsive promoter in normal oral keratinocyte cells (OKF6-TERT) versus HPV(-) UM-SCC-74A or HPV(+) UM-SCC-47 cells treated with either vehicle (DMSO) or forskolin (FSK) and IBMX. Co-transfection with a GFP reporter was used for normalization. Data are presented as the mean \pm SEM ($n = 3$ biologic replicates, 4 technical replicates each; Student's t test; $***p < 0.001$). **(D)** Representative immunofluorescence images of an additional HPV(+) cell line treated with either vehicle (DMSO) or forskolin and IBMX. Cells were stained with hCRTC2 antibody (green), phalloidin (red), and 4',6-diamidino-2-phenylindole (DAPI; blue). Bar, 100 μ m.

Supplementary Figure S3. MEKK1 knockdown does not affect CRTC:CREB-responsive promoter activity in HPV(-) HNSCC cells. **(A)** Quantitative real-time PCR analysis demonstrating knockdown of *MEKK1* using the validated *MEKK1*-targeted shRNA #2 relative to a control shRNA (shNS). Data are representative data of independent biologic replicates presented as the mean \pm SEM (Student's t test; $****p < 0.0001$). **(B)**

Luciferase reporter assay measuring relative fold induction of a 4xCRE CRTC2:CREB-responsive promoter in HPV(-) UM-SCC-11A cells stably transduced with either shNS or shMEKK1 shRNAs and treated with either vehicle (DMSO) or forskolin (FSK) and IBMX. Data are representative data of independent biologic replicates presented as the mean \pm SEM (Student's t test; ns = not significant).

Supplementary Figure S4. CRTC2 knockdown in HPV(+) HNSCC inhibits cell growth and proliferation. **(A)** Representative immunofluorescence images of HPV(+) UM-SCC-47 cells transduced with lentivirus expressing either shNS or shMEKK1 shRNAs. Cells were stained with hCRTC2 antibody (green), phalloidin (red), and 4',6-diamidino-2-phenylindole (DAPI; blue). **(B)** Quantitative real-time PCR analysis demonstrating knockdown of *CRTC2* using a validated adenovirus expressing a CRTC2-targeted shRNA relative to a control shRNA (shNS). Data are presented as the mean \pm SEM ($n = 3$ biologic replicates, 4 technical replicates each; Student's t test; ** $p < 0.01$). **(C)** Luciferase reporter assay measuring relative fold induction of a 4xCRE CRTC2:CREB-responsive promoter in HPV(+) VU-147-T cells transduced with adenovirus expressing either shNS or shCRTC2 shRNAs and treated with either vehicle (DMSO) or forskolin (FSK) and IBMX. Data are presented as the mean \pm SEM ($n = 3$ biologic replicates, 4 technical replicates each; Student's t test; *** $p < 0.001$). **(D)** Cell proliferation assay showing relative confluency of HPV(+) VU-147-T cells transduced with adenovirus expressing either shNS or shCRTC2 shRNAs. The experiment was performed in biologic triplicate ($n = 4$ technical replicates per experiment) with one representative experiment shown (mean \pm SEM; Benjamini-Hochberg pairwise comparisons; ** $p < 0.001$). Data were collected using an IncuCyte live-cell imager; see methods for details.

Declaration of Competing Interest

A.L.A. is a Global Advisory Board member and paid consultant for LG Chem Life Sciences Innovation Center. All other authors declare no potential conflicts of interest.

CRedit authorship contribution statement

Miranda B. Carper: Conceptualization, Data curation, Formal analysis, Investigation, Methodology, Project administration, Supervision, Validation, Visualization, Writing – original draft, Writing – review & editing. **Saumya Goel:** Data curation, Investigation, Validation, Writing – review & editing. **Anna M. Zhang:** Data curation, Investigation, Validation, Writing – review & editing. **Jeffrey S. Damrauer:** Data curation, Formal analysis, Investigation, Methodology, Project administration, Supervision, Validation, Visualization, Writing – review & editing. **Stephanie Cohen:** Methodology, Project administration, Validation, Writing – review & editing. **Matthew P. Zimmerman:** Data curation, Formal analysis, Investigation, Validation, Writing – review & editing. **Gabrielle M. Gentile:** Data curation, Formal analysis, Investigation, Validation, Writing – review & editing. **Kshitij Parag-Sharma:** Data curation, Formal analysis, Investigation, Methodology, Project administration, Validation, Visualization, Writing – review & editing. **Ryan M. Murphy:** Data curation, Formal analysis, Investigation, Validation, Writing – review & editing. **Kotaro Sato:** Data curation, Formal analysis, Investigation, Methodology, Validation, Writing – review & editing. **Kwangok P. Nickel:** Data curation, Investigation, Resources, Validation. **Randall J. Kimple:** Data curation, Formal analysis, Resources, Writing – review & editing. **Wendell G. Yarbrough:** Writing – review & editing. **Antonio L. Amelio:** Conceptualization, Data curation, Formal analysis, Funding acquisition, Project administration, Supervision, Visualization, Writing – original draft, Writing – review & editing.

Funding

This work was supported by NIH/NIDCR T90-DE021986 and NIH/NCI T32-CA211056 (to M.B. Carper), DDS Research Fellowship (to A.M. Zhang), NIH/NIGMS T32GM119999 and NIH/NIDCR F31DE028749 (to R.M. Murphy), University Cancer Research Fund (UCRF; to A.L. Amelio), UNC Lineberger Tier 3 Developmental Award (to A.L. Amelio), and in part by a NIH/NIDCR Developmental Research Program (DRP) Grant from the Yale Head and Neck SPORE P50-DE030707 and NIH/NIDCR R01DE030123 (to A.L. Amelio). This work was also supported in part by the Wisconsin Head and Neck Cancer SPORE grant P50DE026787 (RJK) and the UW Comprehensive Cancer Center Support Grant P30 CA014520 (RJK). The Office of Genomics Research, Lineberger Bioinformatics, Small Animal Imaging, Flow Cytometry, and UNC Pathology Services Cores are supported in part by the NCI Center Core Support Grant 5P30CA016080-42 to the UNC Lineberger Comprehensive Cancer Center.

Acknowledgments

The authors thank Drs. Nana Feinberg and Albert Wielgus of the Pathology Services Core (PSC) for expert technical assistance with histology and immunohistochemical analyses, and members of the Amelio and Yarbrough Labs for helpful discussions, suggestions, and/or scientific review of this manuscript. We thank Drs. Gary Johnson for kindly providing the validated MEKK1 shRNA constructs; Marc Montminy for kindly providing the GFP control, CRTC2, non-specific (shNS) and CRTC2 (shCRTC2) shRNA adenoviruses; Johannes Zuber for kindly providing the pRRL-rtTA3 lentiviral vector; Jim Rheinwald and Matthew Ramsey for kindly providing the normal immortalized oral keratinocyte cell lines; and Thomas Carey for kindly providing the UM-SCC-5, UM-SCC-11A, UM-SCC-14A, UM-SCC-74A, UM-SCC-15, and UM-SCC-25 HNSCC cell lines.

References

- Bray F, Ferlay J, Soerjomataram I, Siegel RL, Torre LA, Jemal A. Global cancer statistics 2018: GLOBOCAN estimates of incidence and mortality worldwide for 36 cancers in 185 countries. *CA Cancer J Clin* 2018;**68**(6):394–424.
- Suh Y, Amelio I, Guerrero Urbano T, Tavassoli M. Clinical update on cancer: molecular oncology of head and neck cancer. *Cell Death Dis* 2014;**5**:e1018.
- Dok R, Nuyts S. HPV positive head and neck cancers: molecular pathogenesis and evolving treatment strategies. *Cancers* 2016;**8**(4).
- Chaturvedi AK, Engels EA, Pfeiffer RM, Hernandez BY, Xiao W, Kim E, et al. Human papillomavirus and rising oropharyngeal cancer incidence in the United States. *J Clin Oncol* 2011;**29**(32):4294–301.
- Cancer Genome Atlas N. Comprehensive genomic characterization of head and neck squamous cell carcinomas. *Nature*. 2015;**517**(7536):576–82.
- Cho JH, Hong WG, Jung YJ, Lee J, Lee E, Hwang SG, et al. Gamma-Ionizing radiation-induced activation of the EGFR-p38/ERK-STAT3/CREB-1-EMT pathway promotes the migration/invasion of non-small cell lung cancer cells and is inhibited by podophyllotoxin acetate. *Tumour Biol* 2016;**37**(6):7315–25.
- Li D, Jin L, Alesi GN, Kim YM, Fan J, Seo JH, et al. The prometastatic ribosomal S6 kinase 2-cAMP response element-binding protein (RSK2-CREB) signaling pathway up-regulates the actin-binding protein fascin-1 to promote tumor metastasis. *J Biol Chem* 2013;**288**(45):32528–38.
- Xiao X, Li BX, Mitton B, Ikeda A, Sakamoto KM. Targeting CREB for cancer therapy: friend or foe. *Curr Cancer Drug Targets* 2010;**10**(4):384–91.
- Tasoulas J, Rodon L, Kaye FJ, Montminy M, Amelio AL. Adaptive transcriptional responses by CRTC coactivators in cancer. *Trends Cancer* 2019;**5**(2):111–27.
- Steven A, Friedrich M, Jank P, Heimer N, Budczies J, Denkert C, et al. What turns CREB on? And off? And why does it matter? *Cell Mol Life Sci* 2020;**77**(20):4049–67.

- [11] Park MH, Lee HS, Lee CS, You ST, Kim DJ, Park BH, et al. p21-Activated kinase 4 promotes prostate cancer progression through CREB. *Oncogene* 2013;**32**(19):2475–82.
- [12] Suarez CD, Deng X, Hu CD. Targeting CREB inhibits radiation-induced neuroendocrine differentiation and increases radiation-induced cell death in prostate cancer cells. *Am J Cancer Res* 2014;**4**(6):850–61.
- [13] Tang F, Tang S, Guo X, Yang C, Jia K. CT45A1 siRNA silencing suppresses the proliferation, metastasis and invasion of lung cancer cells by downregulating the ERK/CREB signaling pathway. *Mol Med Rep* 2017;**16**(5):6708–14.
- [14] Wang X, Ren Y, Zhuang H, Meng X, Huang S, Li Y, et al. Decrease of phosphorylated proto-oncogene CREB at Ser 133 site inhibits growth and metastatic activity of renal cell cancer. *Expert Opin Ther Targets* 2015;**19**(7):985–95.
- [15] Altarejos JY, Montminy M. CREB and the CRTC co-activators: sensors for hormonal and metabolic signals. *Nat Rev Mol Cell Biol* 2011;**12**(3):141–51.
- [16] Gu Y, Lin S, Li JL, Nakagawa H, Chen Z, Jin B, et al. Altered LKB1/CREB-regulated transcription co-activator (CRTC) signaling axis promotes esophageal cancer cell migration and invasion. *Oncogene* 2012;**31**(4):469–79.
- [17] Komiya T, Coxon A, Park Y, Chen WD, Zajac-Kaye M, Meltzer P, et al. Enhanced activity of the CREB co-activator Crtc1 in LKB1 null lung cancer. *Oncogene* 2010;**29**(11):1672–80.
- [18] Schumacher Y, Aparicio T, Ourabah S, Baraille F, Martin A, Wind P, et al. Dysregulated CRTC1 activity is a novel component of PGE2 signaling that contributes to colon cancer growth. *Oncogene* 2016;**35**(20):2602–14.
- [19] Amelio AL, Fallahi M, Schaub FX, Zhang M, Lawani MB, Alperstein AS, et al. CRTC1/MAML2 gain-of-function interactions with MYC create a gene signature predictive of cancers with CREB-MYC involvement. *Proc Natl Acad Sci USA* 2014;**111**(32):E3260–8.
- [20] Musicant AM, Parag-Sharma K, Gong W, Sengupta M, Chatterjee A, Henry EC, et al. CRTC1/MAML2 directs a PGC-1 α -IGF-1 circuit that confers vulnerability to PPAR γ inhibition. *Cell Rep* 2021;**34**(8):108768.
- [21] Sonntag T, Ostojic J, Vaughan JM, Moresco JJ, Yoon YS, Yates JR 3rd, et al. Mitogenic signals stimulate the CREB coactivator CRTC3 through PP2A recruitment. *iScience* 2019;**11**:134–45.
- [22] Siu YT, Ching YP, Jin DY. Activation of TORC1 transcriptional coactivator through MEKK1-induced phosphorylation. *Mol Biol Cell* 2008;**19**(11):4750–4761.
- [23] Saito T, Uzawa K, Terajima M, Shiiba M, Amelio AL, Tanzawa H, et al. Aberrant collagen cross-linking in human oral squamous cell carcinoma. *J Dent Res* 2019;**6**:002203451982871.
- [24] Gao J, Aksoy BA, Dogrusoz U, Dresdner G, Gross B, Sumer SO, et al. Integrative analysis of complex cancer genomics and clinical profiles using the cBioPortal. *Sci Signal* 2013;**6**(269):p11. doi:10.1126/scisignal.2004088.
- [25] Mermel CH, Schumacher SE, Hill B, Meyerson ML, Beroukhi R, Getz G. GISTIC2.0 facilitates sensitive and confident localization of the targets of focal somatic copy-number alteration in human cancers. *Genome Biol* 2011;**12**(4):R41.
- [26] Beroukhi R, Mermel CH, Porter D, Wei G, Raychaudhuri S, Donovan J, et al. The landscape of somatic copy-number alteration across human cancers. *Nature* 2010;**463**(7283):899–905.
- [27] Schon M, Rheinwald JG. A limited role for retinoic acid and retinoic acid receptors RAR α and RAR β in regulating keratin 19 expression and keratinization in oral and epidermal keratinocytes. *J Invest Dermatol* 1996;**107**(3):428–38.
- [28] Dickson MA, Hahn WC, Ino Y, Ronfard V, Wu JY, Weinberg RA, et al. Human keratinocytes that express hTERT and also bypass a p16(INK4a)-enforced mechanism that limits life span become immortal yet retain normal growth and differentiation characteristics. *Mol Cell Biol* 2000;**20**(4):1436–47.
- [29] Kimple RJ, Smith MA, Blitzer GC, Torres AD, Martin JA, Yang RZ, et al. Enhanced radiation sensitivity in HPV-positive head and neck cancer. *Cancer Res* 2013;**73**(15):4791–800.
- [30] Musicant AM, Parag-Sharma K, Gong W, Sengupta M, Chatterjee A, Henry EC, et al. CRTC1/MAML2 directs a PGC-1 α -IGF-1 circuit that confers vulnerability to PPAR γ inhibition. *Cell Reports* 2021;**34**(8):108768.
- [31] Sato K, Parag-Sharma K, Terajima M, Musicant AM, Murphy RM, Ramsey MR, et al. Lysyl hydroxylase 2-induced collagen cross-link switching promotes metastasis in head and neck squamous cell carcinomas. *Neoplasia* 2021;**23**(6):594–606.
- [32] Moffat J, Gruenberg DA, Yang X, Kim SY, Kloepfer AM, Hinkle G, et al. A lentiviral RNAi library for human and mouse genes applied to an arrayed viral high-content screen. *Cell* 2006;**124**(6):1283–98.
- [33] Koo SH, Flechner L, Qi L, Zhang X, Sreter RA, Jeffries S, et al. The CREB coactivator TORC2 is a key regulator of fasting glucose metabolism. *Nature* 2005;**437**(7062):1109–11.
- [34] Conkright MD, Guzman E, Flechner L, Su AI, Hogenesch JB, Montminy M. Genome-wide analysis of CREB target genes reveals a core promoter requirement for cAMP responsiveness. *Mol Cell* 2003;**11**(4):1101–8.
- [35] Sanchez-Céspedes M. The role of LKB1 in lung cancer. *Fam Cancer* 2011;**10**(3):447–53.
- [36] Skoulidis F, Heymach JV. Co-occurring genomic alterations in non-small-cell lung cancer biology and therapy. *Nat Rev Cancer* 2019;**19**(9):495–509.
- [37] Sakamoto KM, Frank DA. CREB in the pathophysiology of cancer: implications for targeting transcription factors for cancer therapy. *Clin Cancer Res* 2009;**15**(8):2583–7.
- [38] Seo H-S, Liu DD, Bekele BN, Kim M-K, Pisters K, Lippman SM, et al. Cyclic AMP response element-binding protein overexpression: a feature associated with negative prognosis in never smokers with non-small cell lung cancer. *Cancer Res* 2008;**68**(15):6065–73.
- [39] Chhabra A, Fernando H, Watkins G, Mansel RE, Jiang WG. Expression of transcription factor CREB1 in human breast cancer and its correlation with prognosis. *Oncol Rep* 2007;**18**(4):953–8.
- [40] Katoh Y, Takemori H, Lin XZ, Tamura M, Muraoka M, Satoh T, et al. Silencing the constitutive active transcription factor CREB by the LKB1-SIK signaling cascade. *FEBS J* 2006;**273**(12):2730–48.
- [41] Leelahavanichkul K, Amornphimoltham P, Molinolo AA, Basile JR, Koontongkaew S, Gutkind JS. A role for p38 MAPK in head and neck cancer cell growth and tumor-induced angiogenesis and lymphangiogenesis. *Mol Oncol* 2014;**8**(1):105–18.
- [42] Schumacher Y, Aparicio T, Ourabah S, Baraille F, Martin A, Wind P, et al. Dysregulated CRTC1 activity is a novel component of PGE2 signaling that contributes to colon cancer growth. *Oncogene* 2015.
- [43] Feng Y, Wang Y, Wang Z, Fang Z, Li F, Gao Y, et al. The CRTC1-NEDD9 signaling axis mediates lung cancer progression caused by LKB1 loss. *Cancer Res* 2012;**72**(24):6502–11.
- [44] Komiya T, Coxon A, Park Y, Chen W-D, Zajac-Kaye M, Meltzer P, et al. Enhanced activity of the CREB co-activator Crtc1 in LKB1 null lung cancer. *Oncogene* 2010;**29**(11):1672–80.
- [45] Chhabra A, Fernando H, Watkins G, Mansel RE, Jiang WG. Expression of transcription factor CREB1 in human breast cancer and its correlation with prognosis. *Oncol Rep* 2007;**18**(4):953–8.
- [46] Cheng JC, Esparza S, Sandoval S, Shankar D, Fu C, Sakamoto KM. Potential role of CREB as a prognostic marker in acute myeloid leukemia. *Future Oncol* 2007;**3**(4):475–80.
- [47] Johannessen CM, Johnson LA, Piccioni F, Townes A, Frederick DT, Donahue MK, et al. A melanocyte lineage program confers resistance to MAP kinase pathway inhibition. *Nature* 2013;**504**(7478):138–42.
- [48] Du K, Montminy M. CREB is a regulatory target for the protein kinase Akt/PKB. *J biolog Chem* 1998;**273**(49):32377–9.
- [49] Quinn PG. Distinct activation domains within cAMP response element-binding protein (CREB) mediate basal and cAMP-stimulated transcription. *J biolog Chem* 1993;**268**(23):16999–7009.
- [50] Xing J, Kornhauser JM, Xia Z, Thiele EA, Greenberg ME. Nerve growth factor activates extracellular signal-regulated kinase and p38 mitogen-activated protein kinase pathways to stimulate CREB serine 133 phosphorylation. *Mol Cell Biol* 1998;**18**(4):1946–55.

- [51] Zhang X, Odom DT, Koo SH, Conkright MD, Canettieri G, Best J, et al. Genome-wide analysis of cAMP-response element binding protein occupancy, phosphorylation, and target gene activation in human tissues. *Proc Natl Acad Sci USA* 2005;**102**(12):4459–64.
- [52] Rodon L, Svensson RU, Wiater E, Chun MGH, Tsai WW, Eichner LJ, et al. The CREB coactivator CRTC2 promotes oncogenesis in LKB1-mutant non-small cell lung cancer. *Sci Adv* 2019;**5**(7):eaaw6455.
- [53] Zhou X, Li JW, Chen Z, Ni W, Li X, Yang R, et al. Dependency of human and murine LKB1-inactivated lung cancer on aberrant CRTC-CREB activation. *eLife* 2021;10.
- [54] Uebi T, Tamura M, Horike N, Hashimoto YK, Takemori H. Phosphorylation of the CREB-specific coactivator TORC2 at Ser(307) regulates its intracellular localization in COS-7 cells and in the mouse liver. *Am J Physiol Endocrinol Metab* 2010;**299**(3):E413–25.
- [55] Wang Y, Liu Q, Zhang H. Phosphorylation of CREB-specific coactivator CRTC2 at Ser238 Promotes proliferation, migration, and invasion of colorectal cancer cells. *Technol Cancer Res Treat* 2020;**19**:1533033820962111.
- [56] Leelahavanichkul K, Amornphimoltham P, Molinolo AA, Basile JR, Koontongkaew S, Gutkind JS. A role for p38 MAPK in head and neck cancer cell growth and tumor-induced angiogenesis and lymphangiogenesis. *Mol Oncol* 2014;**8**(1):105–18.
- [57] Satsuka A, Mehta K, Laimins L. p38MAPK and MK2 pathways are important for the differentiation-dependent human papillomavirus life cycle. *J Virol* 2015;**89**(3):1919–24.
- [58] Lali FV, Hunt AE, Turner SJ, Foxwell BM. The pyridinyl imidazole inhibitor SB203580 blocks phosphoinositide-dependent protein kinase activity, protein kinase B phosphorylation, and retinoblastoma hyperphosphorylation in interleukin-2-stimulated T cells independently of p38 mitogen-activated protein kinase. *J Biol Chem* 2000;**275**(10):7395–402.
- [59] Dentin R, Hedrick S, Xie J, Yates J 3rd, Montminy M. Hepatic glucose sensing via the CREB coactivator CRTC2. *Science* 2008;**319**(5868):1402–5.
- [60] Zeng Q, Chen J, Li Y, Werle KD, Zhao RX, Quan CS, et al. LKB1 inhibits HPV-associated cancer progression by targeting cellular metabolism. *Oncogene* 2017;**36**(9):1245–55.
- [61] Hu Y, Wu MZ, Gu NJ, Xu HT, Li QC, Wu GP. Human papillomavirus 16 (HPV 16) E6 but not E7 inhibits the antitumor activity of LKB1 in lung cancer cells by downregulating the expression of KIF7. *Thorac Cancer* 2020;**11**(11):3175–80.
- [62] Yang JH, Li XY, Wang X, Hou WJ, Qiu XS, Wang EH, et al. Long-term persistent infection of HPV 16 E6 up-regulate SP1 and hTERT by inhibiting LKB1 in lung cancer cells. *PLoS one* 2017;**12**(8):e0182775.
- [63] Yang JH, Wu MZ, Wang XB, Wang S, Qiu XS, Wang EH, et al. HPV16 E6/E7 upregulate hTERT mRNA and gene amplification levels by relieving the effect of LKB1 on Sp1 phosphorylation in lung cancer cells. *Ther Adv Med Oncol* 2020;**12**:1758835920917562.
- [64] Carper MB, Troutman S, Wagner BL, Byrd KM, Selitsky SR, Parag-Sharma K, et al. An immunocompetent mouse model of HPV16(+) head and neck squamous cell carcinoma. *Cell Rep* 2019;**29**(6) 1660–74 e7.